Carbon 203 (2023) 876–885

Contents lists available at ScienceDirect

Carbon

journal homepage: www.elsevier.com/locate/carbon

Waste plastic- and coke-derived flash graphene as lubricant additives

Paul A. Advincula [a], Victoria Granja [b], Kevin M. Wyss [a], Wala A. Algozeeb [a], Weiyin Chen [a], Jacob L. Beckham [a], Duy Xuan Luong [a], C. Fred Higgs III [b,c,**], James M. Tour [a,d,e,*]

[a] Department of Chemistry, USA
[b] Department of Mechanical Engineering, USA
[c] Department of Bioengineering, USA
[d] Department of Materials Science and NanoEngineering, USA
[e] Smalley-Curl Institute, NanoCarbon Center, and the Welch Institute for Advanced Materials, Rice University, 6100 Main Street, Houston, TX, 77005, USA

ARTICLE INFO

Keywords:
Flash graphene
Lubricant additives
Waste plastic
Metallurgical coke

ABSTRACT

Lubricants play an essential role in reducing wear in mechanical systems. Carbon nanomaterial additives, such as graphene, have been found to significantly improve tribological performance when used as lubricant additives. Here, post-consumer plastic and metallurgical coke are converted into turbostratic flash graphene (FG) through flash Joule heating (FJH). The FG is then added to either poly(alpha olefin) 6 or 9 (PAO 6 or PAO 9). Adding waste plastic-derived FG (WPFG) and metallurgical coke-derived FG (MCFG) to lubricants resulted in a significant decrease in the coefficient of friction (CoF), wear scar diameter (WSD), and roughness during four-ball testing. WPFG and MCFG decrease the CoF in PAO 9 by 6% and 9% at 0.1 mg mL^{-1}, respectively, and in PAO 6 by 23% and 6% at 0.5 mg mL^{-1}, respectively. WPFG and MCFG decrease the WSD of steel balls in PAO 9 by 14% and 8% at 0.5 mg mL^{-1}, respectively, and in PAO 6 by 12% and 14% at 0.5 mg mL^{-1}, respectively, by forming a coating-like layer between the metal surfaces. Roughness decreased by 38% and 32% for WPFG and MCFG in PAO 6, respectively, and by 35% and 29% for WPFG and MCFG in PAO 9, respectively. Finally, preliminary life cycle analyses demonstrate that production of FG produces up to 99% less greenhouse gas emissions, requires 98% less energy, and consumes 99.9% less water when compared to conventional production techniques of graphene. Hence, metallurgical coke and waste plastic are shown to be ready feedstocks for high-quality FG lubricant additives.

1. Introduction

Friction is a significant contributor to global CO_2 emissions since a large amount of energy is lost overcoming friction in mechanical systems. The energy required to do this is often derived from non-renewable energy resources such as petroleum. Additionally, high friction can lead to higher wear rates of the parts in contact, reducing their lifetime and reliability. Lubricants, particularly liquid lubricants, are a longstanding solution for reducing the friction between surfaces. The use of carbon nanomaterials like graphene [1] as additives in the liquid lubricants aids reduction in the coefficient of friction (CoF) and also protects the surfaces in sliding contact by forming a protective layer over the surfaces in contact and by smoothing the interacting layers. It is presumed that the graphene prevents direct contact of the mechanical surfaces thereby also reducing the wear scar diameter (WSD).

Graphene consists of a honeycomb sheet of carbon atoms, resulting in a structure with outstanding thermal, mechanical, and electrical properties. The high cost of production has so far limited the application of graphene at larger scales. Recently, we demonstrated a rapid and inexpensive process for converting carbon-containing feedstocks [2–4], including plastics [5], rubber [6], and plastic pyrolysis ash [7], into high-quality, turbostratic flash graphene (tFG) through flash Joule heating (FJH). The scaleup of the FJH process could produce enough FG to be used as an inexpensive lubricant additive in commercial products [8]. When compared to reduced graphene oxide synthesized using the modified Hummer's method, tFG products are more oxidatively stable [9].

Upcycling of waste plastic is of significant interest as plastic pollution

* Corresponding author. Smalley-Curl Institute, NanoCarbon Center, and the Welch Institute for Advanced Materials, Rice University, 6100 Main Street, Houston, TX, 77005, USA.
** Corresponding author. Department of Mechanical Engineering, USA.
E-mail addresses: higgs@rice.edu (C.F. Higgs), tour@rice.edu (J.M. Tour).

https://doi.org/10.1016/j.carbon.2022.12.035
Received 25 October 2022; Received in revised form 9 December 2022; Accepted 11 December 2022
Available online 12 December 2022

is rapidly becoming one of the world's most urgent environmental concerns [10]. Production of plastics results in significant greenhouse gas emissions [11]. By 2050, plastic production will increase to >1,000 Mt and account for 20% of global oil consumption [12]. Most end-of-life waste plastic is relegated to landfills or the ocean, slowly decomposing to micro- and nano-plastics, threatening microorganisms [13], bacteria [14], marine life [15], and humans [16,17]. Half of Earth's oxygen is provided by the ocean [18], mostly produced by plankton. Normally, these organisms capture carbon through photosynthesis, but increasing amounts of microplastics affect their ability to sequester carbon and further accelerate the loss of ocean oxygen [19,20]. As such, upcycling of waste plastic into a lubricant additive is both economically and environmentally advantageous.

Similarly, coal-based feedstocks are particularly advantageous for upcycling as the annual consumption of coal is estimated to decrease from 5.25 billion tons to 600 million tons from 2020 to 2050. This is due to the growth of renewable energy sources, including solar and wind power [21]. As a result, new applications for coal materials are continually being sought. Coals vary in composition and properties, depending on the type. Several different grades, including anthracitic coal, charcoal, calcined coke, and petroleum coke, have been successfully converted into FG [22]. Metallurgical coke has emerged as one of the best coal-derived feedstocks for FJH because of its high carbon content, conductivity, and purity [23,24].

In this work, tFG upcycled from waste plastic and metallurgical coke is used as a lubricant additive. This work demonstrates that the turbostratic characteristics of tFG aids its dispersion in PAO 6 and PAO 9, reducing the CoF, surface roughness, and WSD of the lubricants in four-ball tribology tests. Previous reports of turbostratic graphite as oil additives did not show a statistically significant decrease in CoF [25]. Turbostratic graphene is shown here for the first time as an additive to lubricants. AB-stacked graphene has generally required extensive chemical modification or addition of surfactants to enhance its dispersibility, but turbostratic graphene does not require further modification to be dispersed in lubricant oil. PAO is a synthetic hydrocarbon with a structure like that of mineral oil and is used extensively in automotive fluids, hydraulic oils, and gear oils. Given the projected low cost and high performance of tFG as a lubricant additive, it might offer advantages over current additives.

2. Experimental

2.1. Materials

Waste plastic flash graphene (WPFG) was prepared by shredding post-consumer high-density polyethylene (HDPE). Carbon black (CB, BP-2000, 5 wt%) was purchased from Cabot Corporation and added to the shredded HDPE to increase the conductivity of the plastic. The blend of 5% CB:HDPE was subjected to AC pretreatment for 8 s in a FJH system, before being flashed at 120 V for 500 ms, resulting in WPFG, similar to our published protocol. [5] Metallurgical coke flash graphene (MCFG) was prepared by flash Joule heating #12-20 metallurgical coke (MC) obtained from SunCoke Energy. The MC sample was subjected to a variable FJH pulse with duty cycles of 10% for 1s, 20% for 0.5 s, and 50% for 5s, and 1k Hz frequency, resulting in MCFG. Pulses of 370 V were used. The MCFG was then ball milled with steel balls at a weight ratio of 100:15 steel balls:MCFG for 2 h at 400 rpm. Synfluid PAO 9 cSt (Batch: DCS-113018) was obtained from Chevron Phillips and used as received. Synfluid PAO 6 cSt (Batch: DCS-111219) was obtained from Chevron Phillips and used as received. Commercial graphene (CG) was obtained from Tianyuan Empire Materials & Technology Limited.

2.2. Raman spectroscopy analysis

Raman spectra were collected using a Renishaw inVia confocal Raman microscope with 532 nm excitation. Large-area Raman mapping was used to assess the bulk crystallinity and nanostructure of the graphene resulting from individual flashes. Raman maps were analyzed using a custom-written Python script employing the RamPy package. Spectra were background-corrected and smoothed using a Savitsky-Golay filter prior to the quantification of graphene yield and peak ratios. Spectra with a I_{2D}/I_G ratio of $\geq$0.3, a signal-to-noise ratio of >5 in the 2D band region, and a 2D band FWHM of <100 cm^{-1} were classified as graphene.

2.3. X-ray photoelectron spectroscopy (XPS)

XPS data was collected using a PHI Quantera SXM Scanning X-ray microprobe maintained at 5×10^{-9} Torr. Survey spectra were recorded with a step size of 0.5 eV at a pass energy of 140 eV. Elemental spectra were collected using a 0.1 eV step size at a pass energy of 26 eV. Peak fitting was carried out using a Shirley baseline correction.

2.4. X-ray diffraction spectroscopy (XRD)

XRD data was collected on samples ground with a mortar and pestle and analyzed on a Rigaku SmartLab II instrument using zero background sample holders. A scan width of 0.02° $step^{-1}$ and scan rate of 2° min^{-1} was used.

2.5. UV–vis spectroscopy

A UV–vis spectrometer (Shimadzu UV-3600 Plus configured with a photomultiplier tube from 200 to 1000 nm wavelength) was used to collect the spectra of suspensions of CG, MCFG, and WPFG in PAO 6 and PAO 9. Each type of graphene (0.5–4 mg mL-1) was added to PAO 6 and PAO 9. The mixture was sonicated (Cole-Parmer 750-W ultrasonic processor with a cup horn) for 30 min to obtain a dispersion. The mixture was centrifuged (Clay Adams Analytical Centrifuge CT-3201) for 30 min at 3200 rpm. The supernatant was analyzed by UV–vis spectroscopy. The absorbance was recorded at 660 nm. An extinction coefficient of α_{660} = 6,600 L g^{-1} m^{-1} was used to calculate the concentration of carbon materials in the aqueous solution [22].

2.6. Transmission electron microscopy (TEM)

Samples of FG were imaged by drop-casting diluted solutions (~1 mg mL^{-1} in ethanol) of FG (<300 μL) onto a 200 mesh Cu grid with lacey carbon. This dilute solution was sonicated (Cole-Parmer 750-W ultrasonic processor with a cup horn) for 15 min prior to drop-casting. A JEOL 2100F field-emission gun TEM at 200 kV was used to image the samples.

2.7. Four-ball testing

The tribological performance of the solutions was evaluated in terms of the CoF and anti-wear properties using a four-ball tester. A rotating steel ball is pressed against three stationary lower balls fully immersed in the lubricant being tested (Fig. S1). In the lubricant industry, this technique is widely used in the evaluation of lubricating oils designed to operate under severe conditions. The test conditions were set in accordance with the ASTM standard D4172-B [26]. The temperature of the test lubricant was regulated at 75 °C and the applied load at 40 kgf (392 N). Once these conditions were reached and maintained constant, the upper ball was rotated at 1200 rpm for 60 min. The balls used for this study were made from AISI chrome steel E−52100 and have a diameter of 12.7 mm with Grade 25 Extra Polish (EP). The test balls, test-lubricant cup, and chuck assemblies were thoroughly cleaned before and after each test by first washing them with cleaning solvent (acetone, ACS Reagent ≥99.5%) and then a rinse solvent (ASTM n-heptane).

PAO 9 and PAO 6 were used as the base lubricants where WPFG and MCFG were added at different concentrations. All solutions were

sonicated (Cole-Parmer 750-W ultrasonic processor with a cup horn) for 15 min before the tests to produce a good dispersion. The CoF of each solution is measured as a function of time for the duration of the test. The average values of the CoF for the solutions of PAO 6 or PAO 9 with FG are reported.

WSD is another measurement to quantify the tribological performance of a lubricant. WSD is obtained by measuring the diameters of the scars produced on the lower three stationary balls as shown in Fig. S2. Two measurements are taken for each ball. The first measurement is along a radial line from the center of the holder and the second along a line 90° from the first measurement. The WSD is reported as the arithmetic average of these six measurements.

White light interferometry (WLI) was used to measure the surface roughness of the balls used in the tests. The average surface roughness (Ra) of the balls was found to be 126 nm, which is a very smooth engineering surface (Fig. S3).

Hamrock and Dowson's elastohydrodynamic film thickness equations [27] were used to predict the central and minimum film thicknesses of the lubricant mixtures. The *lambda* ratio (ratio of the lubricant film thickness to the composite surface roughness) was then calculated indicating that the system operates in the boundary lubrication regime. This regime suggests that the friction is primarily due to the surfaces being in sliding contact.

2.8. Scanning electron microscopy (SEM) and energy dispersive X-ray spectroscopy (EDS)

SEM images and EDS spectra of the wear scars after tribological testing were obtained using a high-resolution field emission scanning electron microscope (FEI Quanta 400 ESEM FEG). The SEM images were captured at 600x magnification with a dwell time per pixel of 60 μs and an 11.3 mm working distance in high vacuum. The electron landing energy was 15 kV using the through lens detector in the back scatter electron detection mode. The EDS spectra were recorded at the same conditions as the SEM images with a resolution of 131.3 eV and amp time of 7.68 μs.

3. Results and discussion

Samples of WPFG and MCFG were prepared by FJH of WP and MC, respectively. As shown in Fig. 1, these samples were then mixed with PAO 9 or PAO 6 through cup-horn sonication prior to tribological testing. As a qualitative test of dispersion stability, CG, MCFG, and WPFG in PAO 6 and PAO 9 were left to settle for 1 week with a concentration of 4 mg mL^{-1} (Fig. S4). CG was found to be the least stable of the samples. MCFG and WPFG were both stable throughout the 1-week period. Four-ball testing was used to examine the properties of the FG-modified lubricants under high contact loads.

A variety of characterization methods are used to analyze the quality of FG produced through FJH, including Raman, XRD, and XPS, as seen in Fig. 2. Raman spectroscopy is a commonly used technique for determining the quality and morphology of graphene through analysis of the characteristic Raman peaks that appear at ~1350, ~1580, and ~2700 cm^{-1} (D, G, and 2D, respectively). In Fig. 2a, the average spectrum of 100 different spectra is presented, along with the standard deviation shown by the shaded regions. Spectra meeting the following criteria were classified as FG: (1) a I_{2D}/I_G ratio of ≥0.3, (2) a signal-to-noise ratio of >5 in the 2D band region, and (3) a 2D band FWHM of <100 cm^{-1}. The feedstocks for WPFG and MCFG, which are 5% CB: HDPE and MC, have low average I_{2D}/I_G ratios of 0.198 and 0.109, respectively. These ratios, combined with the high I_D/I_G ratios of 0.790 and 0.835 for 5% CB:HDPE and MC, respectively, indicated that these starting feedstocks are amorphous and do not contain FG. After FJH, the average I_{2D}/I_G ratios for WPFG and MCFG increase to 0.895 and 0.557, respectively. The I_D/I_G ratios correspondingly decrease to 0.540 and 0.474 for WPFG and MCFG, respectively. The high average I_{2D}/I_G ratio indicates that the graphene is good quality, while the standard deviation shows that each sample is relatively homogeneous. Process yields of WPFG and MCFG are ~40% and >95%, respectively. Process yield is defined here as the mass of the product measured against the mass of the feedstock. CG was found to have an average I_{2D}/I_G and I_D/I_G ratio have 0.394 and 0.054, respectively, with a graphene yield of 98.9%. CG is indeed good quality graphene with a very low concentration of defects, as indicated by the low I_D/I_G ratio.

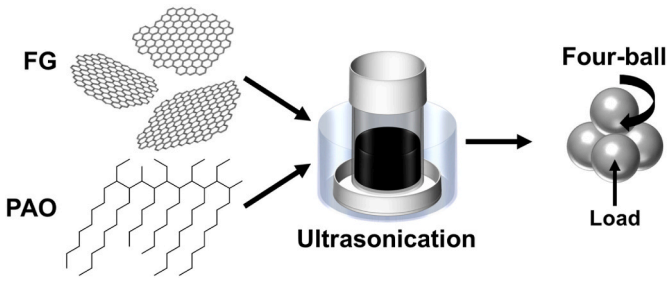

Fig. 1. Schematic depicting the addition and ultrasonication of WPFG or MCFG into PAO 9 and PAO 6. These solutions are subsequently used as lubricants in four-ball tribometry tests. (A colour version of this figure can be viewed online.)

The XPS surveys shown in Fig. 2b for 5% CB:HDPE, WPFG, MC, MCFG, and CG show high carbon composition. 5% CB:HDPE and WPFG have no detectable heteroatoms. While both MC and MCFG have oxygen present, after FJH the oxygen proportion drops from 8.2 to 5.5%, while silicon is reduced below the detection limit, indicating that MCFG is a higher-purity carbon material than the MC starting material. High-resolution carbon XPS of the samples show large C–C and C═C peaks occurring at ~284.8 eV (Fig. S5). MC and MCFG also show C–O and O–C═O peaks at ~286.33 and ~288.71 eV, respectively. These samples possess oxygen peaks at ~531.42 and ~533.93 eV, which correspond to R-C-O and R-C═O bonds, respectively (Fig. S6).

Analysis of the Raman spectra obtained during characterization yields the data shown in Fig. 2c. Here, WPFG and MCFG are found to have high FG yields, indicating that the starting feedstocks are successfully and efficiently converted into FG. 100 spectra are collected for each set of maps, providing a representative sample of the FG. The yield is determined by the percentage of the 100 spots having the minimum standard for the three criteria described above for Fig. 2a. This is not the mass-to-mass conversion yield. XPS surveys show that carbon makes up most non-hydrogen atoms present in CG, WPFG, MCFG, and the feedstocks for conversion. Combined, these characterization techniques confirm that WP and MC can be converted into high-quality FG.

The XRD of WPFG and MCFG confirm that the FG samples are turbostratic, meaning that there is rotation of the graphene layers about the axis normal to the graphene layers, as well as increased interlayer spacing. Fig. 3a shows that the (002) peaks of each FG sample have an increased FWHM and decreased diffraction angle when compared to CG and graphite nanoplatelets in our previous work [6], indicating increased interlayer spacing in FG. The small FWHM and increased diffraction angle of CG indicates that CG is AB-stacked. The XRD also shows reduced three-dimensional peaks, such as the (101) and (102) peaks, in the samples of FG. The decrease in intensity of these three-dimensional lines is indicative of graphene layer rotation [28]. The 5% CB:HDPE feedstocks possesses characteristic HDPE peaks at 21.7° and 24.1°, which are not visible in WPFG, indicating complete conversion of the material. The (002) peak of MC is significantly broader than that of MCFG, demonstrating that the MC is amorphous when compared to MCFG. The turbostraticity observed in WPFG and MCFG makes these materials preferable for lubricant additives since the reduced van der Waals interactions from layer rotation and increased interlayer spacing between sheets should make them easier to exfoliate in lubricants under shear.

The improvement in dispersibility is clearly demonstrated through

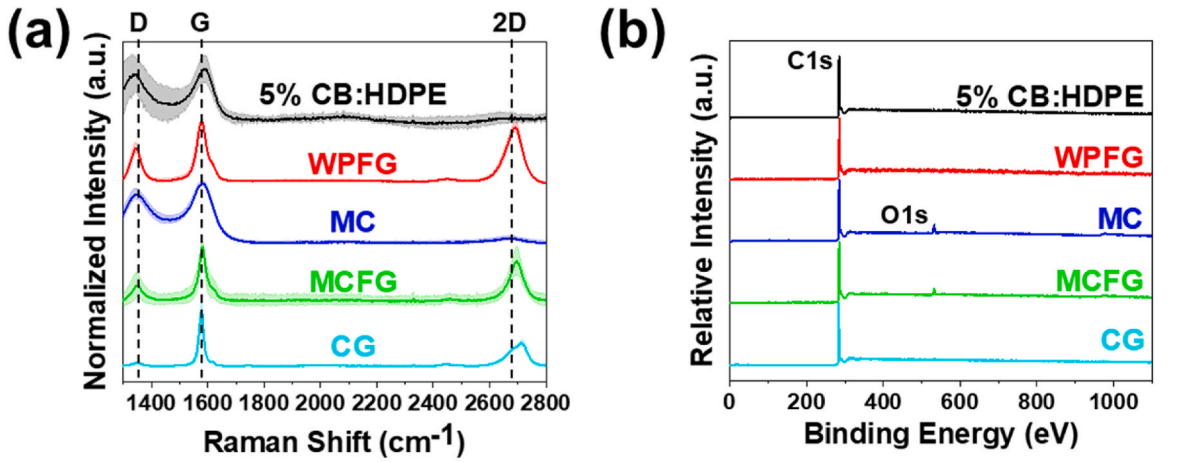

(c)

Sample:	Avg. I_{2D}/I_G Ratio:	Avg. I_D/I_G Ratio:	Graphene Yield (%):	C (%):	O (%):	Si (%):
5% CB:HDPE	0.198	0.790	N/A	>99%	<1%	<1%
WPFG	0.895	0.540	>99	>99%	<1%	<1%
MC	0.109	0.835	N/A	90.6	8.2	1.2
MCFG	0.794	0.343	96.9	94.3	5.5	<1%
CG	0.394	0.054	98.9	97.8	2.0	<1%

Fig. 2. (a) Average Raman spectra with standard deviation shown by shaded regions (N = 100). The dashed lines indicate the positions of the D, G, and 2D peaks in the average Raman spectrum of WPFG, MCFG, their feedstocks, and CG. (b) XPS surveys of WPFG, MCFG, their feedstocks, and CG. (c) Yield, intensity ratios, and elemental analyses for characterization of MCFG and WPFG after FJH conversion, as well as CG. NA means not applicable. (A colour version of this figure can be viewed online.)

UV–vis spectroscopy. After sonication and centrifugation, the final concentrations of WPFG and MCFG are much higher than CG, in both PAO 6 and PAO 9. In PAO 6, the final concentrations of WPFG and MCFG are on average 8x and 4x that of CG, respectively (Fig. 3b and c). In PAO 9, the final concentrations of WPFG and MCFG are on average 14x and 5x that of CG, respectively (Fig. 3d and e). The turbostraticity of FG materials renders them much more dispersible than AB-stacked FG in lubricant oil, making them an ideal candidate for addition to lubricants.

These results show that addition of FG enhances the tribological performance of PAO 9. The lowest CoF is obtained at a concentration of 0.1 mg mL^{-1} FG in PAO 9, reducing the CoF by 6% and 9% compared with the base oil when using WPFG and MCFG, respectively (Fig. 4a). Beyond this point, CoF gradually increases as the graphene loading increases. This indicates that the graphene loading likely exceeded a critical value, leading to discontinuity in the oil film and dry friction [29]. In contrast, the WSD decreases dramatically with increasing FG concentration up to 0.5 mg mL^{-1} (Fig. 4b). At this concentration, the WSD is reduced by 14% for WPFG and by 8% for MCFG as compared with pure PAO 9.

Similar improvement in tribological performance with the addition of FG is observed with PAO 6. Here, the minimum CoF is obtained at a concentration of 0.5 mg mL^{-1} FG in PAO 6, with a reduction of 23% and 6% in comparison to the base oil when WPFG and MCFG are added, respectively (Fig. 4c). Here, the increase of CoF with higher concentration is not observed as it was with PAO 9. WSD decreases as before, up to the maximum concentration of 0.5 mg mL^{-1}. At this point, WSD decreases by 12% for WPFG and 14% for MCFG (Fig. 4d). These results indicate that adding turbostratic graphene improves the anti-wear properties of PAO 9 and PAO 6.

SEM and EDS elemental analysis were performed (Fig. S7 and Fig. S8) to further elucidate the lubrication mechanism of FG. It was found that the chemical composition of the wear scar changed when FG was used as an additive as compared to the chemical composition of the wear mark when using base oils alone. This change in composition indicates that FG did have an effect on the tribolayer formed during the tests. The spectral analysis of the worn surface shows that carbon was introduced into the tribolayer when using FG as an additive.

When comparing the chemical composition of the tribolayer formed after the tribological tests for the same concentration (0.5 mg mL^{-1}) of WPFG and MCFG in PAO 9 (Fig. S7), it was noted that MCFG produced a larger change in the content of carbon of the tribolayer than WPFG. In the case of PAO 6 (Fig. S8), the opposite is true, which means that for the same concentration (0.5 mg mL^{-1}), the content of carbon in the tribolayer is larger when using WPFG. For PAO 9 and PAO 6, the best performing samples in terms of WSD (i.e., 0.5 mg mL^{-1} WPFG in PAO 9 and 0.5 mg mL^{-1} MCFG in PAO 6) are the ones with lower percentages of carbon using 0.5 mg mL^{-1} loadings of FG as additive. For PAO 6 and PAO 9, the best performing samples in terms of CoF are the ones with a carbon content of ~1 wt%.

Additionally, from the SEM figures, almost no signs of abrasive wear

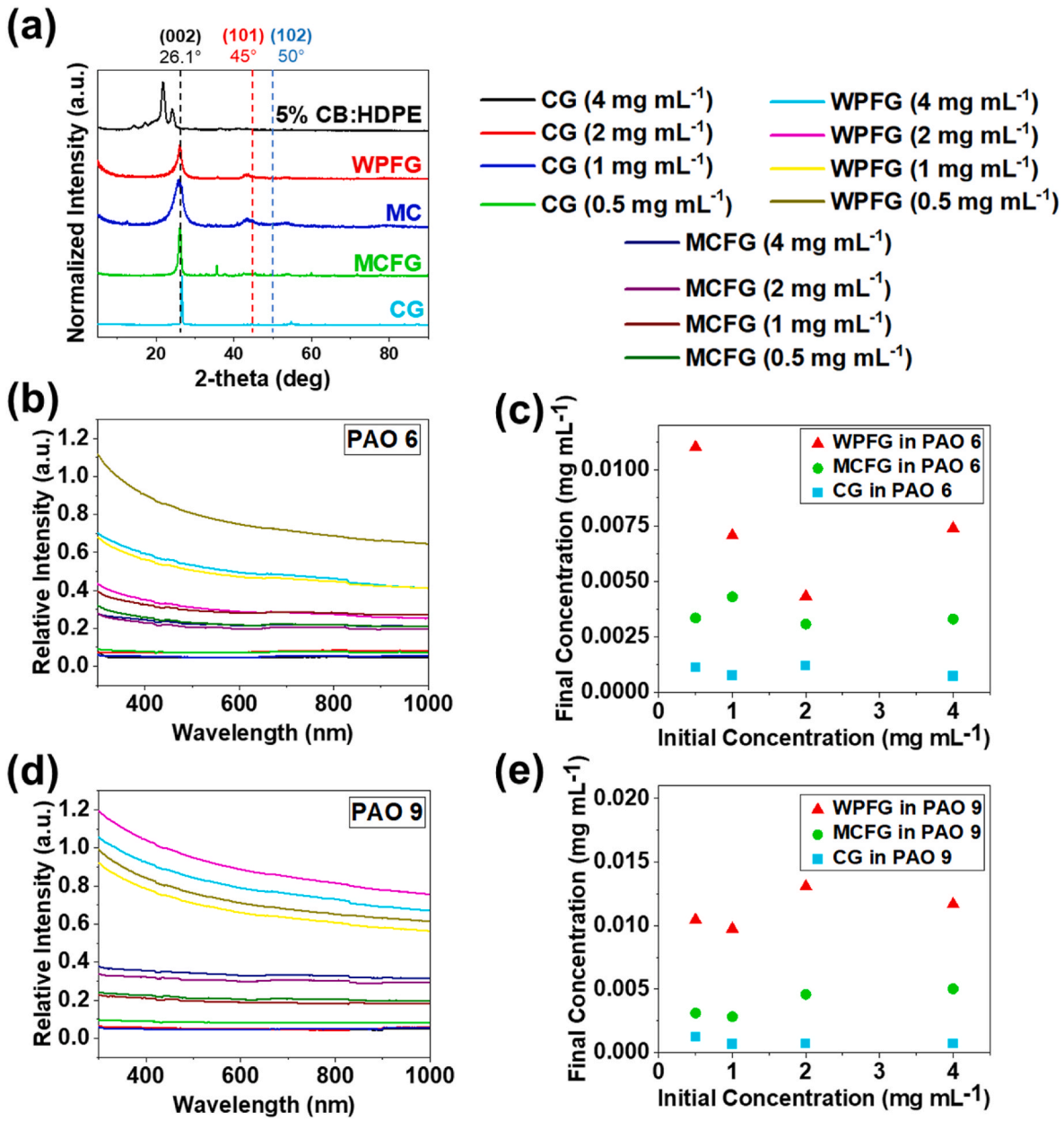

Fig. 3. (a) XRD patterns of WPFG, MCFG, their feedstocks, and CG. The dashed lines indicate the positions of the (002), (101), and (102) peaks in the XRD patterns. (b) UV–vis measurements and (c) initial/final concentrations of WPFG, MCFG, and CG in PAO 6. (d) UV–vis measurements and (e) initial/final concentrations of WPFG, MCFG, and CG in PAO 9. (A colour version of this figure can be viewed online.)

are present in the best performing samples in terms of WSD and that the grooves for these samples are shallower than the grooves of the wear scar obtained when using the base oils alone. This indicates that FG had a smoothing effect in the samples, moving the lubrication regime to the hydrodynamic regime, characterized by lower wear. This effect will be further explored by measuring the roughness of the wear marks using white light interferometry.

From the spectral analysis of the wear scars (Fig. S7e and Fig. S8e) it is also inferred that the chemical composition of the base oils affects the chemical composition of the tribolayer. The difference in lubrication performance between PAO 6 and PAO 9 can be attributed to this difference in chemical composition.

As predicted by Hamrock and Dowson equations (See Supporting Information), the system operated in the boundary lubrication regime. Within this range of operation, the bulk properties of the lubricant (such as density and viscosity) are not as important as the chemical properties of the lubricant and the properties of the substrates in contact [30]. Therefore, the decrease in WSD as a function of concentration can be mainly attributed to the formation of a protective film at the contact interface. It has been demonstrated that when using graphene as a lubricant additive, it can deposit on the friction interface to form a protective film [1,31,32]. This stable tribo-layer prevents direct contact between the solid surfaces, and provides an extremely low shear strength, thereby enhancing the reduction of friction and wear [33–35].

Additionally, low friction solids, such as FG, can also have a smoothing effect on the interacting surfaces by filling in grooves and/or scars. In doing so, the surface roughness effectively decreases, and lambda increases, indicating the possibility for movement to the mixed and hydrodynamic lubrication regimes (Fig. S9), which are characterized by reduced wear behavior [30].

To elucidate the effect of FG on the surface roughness of the point of contact, a series of roughness measurements were performed on the

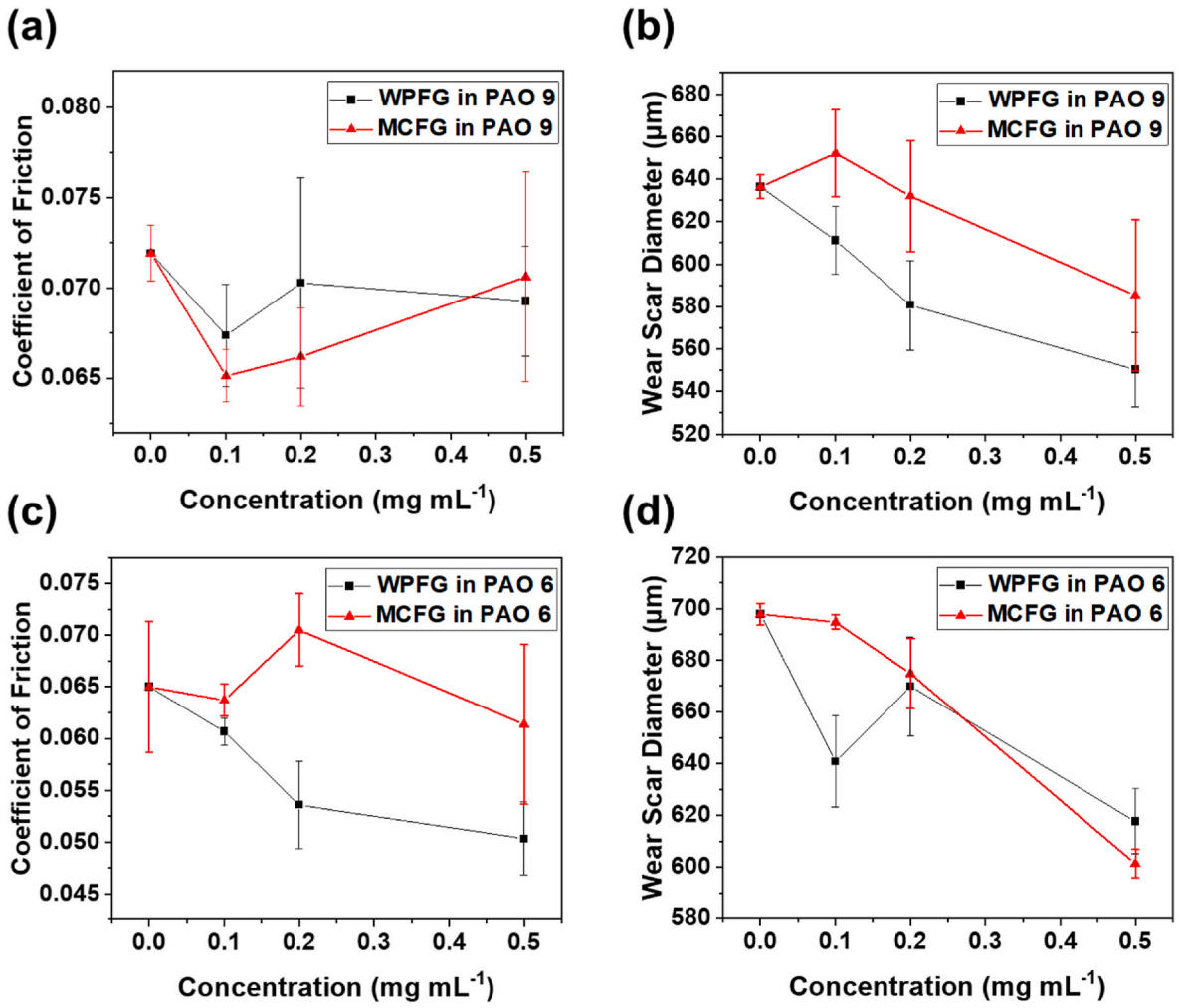

Fig. 4. (a) Average CoF of 1 h tests of PAO 9 compounded with WPFG and MCFG. (b) Average WSD for varying concentrations of WPFG and MCFG in PAO 9, after 1 h of testing. (c) Average CoF over 1 h tests of PAO 6 compounded with WPFG and MCFG. (d) Average WSD for varying concentrations of WPFG and MCFG in PAO 6, after 1 h of testing. The error bars represent one standard error (N = 3). The first data point is representative of the PAO base oil alone. (A colour version of this figure can be viewed online.)

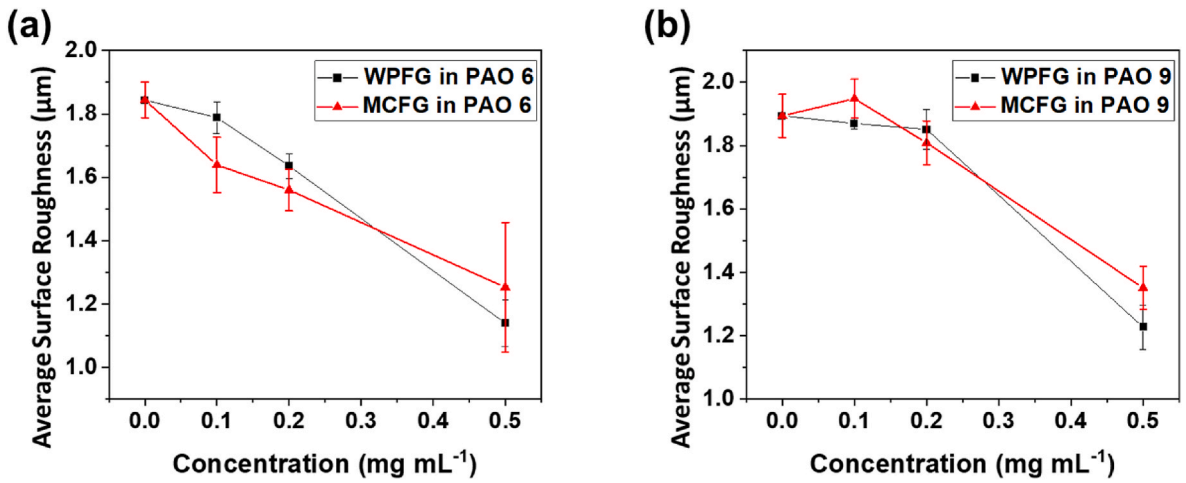

Fig. 5. Average roughness of wear scars measured using WLI at 20x after 1 h tests and after sonicating the balls for 30 min in an acetone bath. Average values for (a) PAO 9 compounded with FG and (b) PAO 6 compounded with FG. The error bars represent one standard error (N = 3). (A colour version of this figure can be viewed online.)

wear scars after the 1 h tests. The balls were ultrasonically cleaned for 30 min in an acetone bath. The roughness of the samples was then measured at 20x and reported for each base lubricant and concentration of FG.

Fig. 5 shows that surface roughness of the wear scar after testing the samples with PAO 9 and PAO 6 compounds was dramatically reduced with the addition of FG. At 0.5 mg mL^{-1}, roughness decreased by 38% and 32% for WPFG and MCFG in PAO 6, respectively, and by 35% and 29% for WPFG and MCFG in PAO 9, respectively. These results agree with previous studies in which enhanced lubrication performance due to the graphene-family materials in liquid lubrication has been attributed to: (i) a ball-bearing mechanism, where graphene particles act like rolling elements and reduce friction; (ii) a self-repairing mechanism, where the graphene fills in the valleys within the surface topography; (iii) and a surface polishing mechanism where the graphene polishes asperity tips rendering the surfaces more smooth, thereby reducing the friction and/or enabling the antiwear performances [33,36].

Fig. 6 show that the friction surfaces tested with pure base oils PAO 6 and PAO 9 have deeper furrows than the friction interface tested with 0.5 mg mL^{-1} FG solution. Representative images of the surfaces of pure PAO 6 and PAO 9 have roughness measurements at 20x of 1.779 μm and 1.958 μm, respectively. The addition of WPFG to PAO 6 and PAO 9 at a concentration of 0.5 mg mL^{-1} results in the greatest reduction in roughness to 1.055 μm and 1.156 μm, respectively. The addition of MCFG to PAO 6 and PAO 9 reduce roughness to 1.379 μm and 1.428 μm, respectively. It is evident that the addition of FG smoothed the surface, reducing surface roughness.

In this study, higher FG concentration translates into enhanced tribological performance in terms of wear. However, the existing literature reports that once this concentration surpasses a threshold, the graphene will start to stack and agglomerate between friction pairs [29], hindering the tribological performance of the lubricant (i.e., degrading the antiwear properties and finally leading to dry friction) since this causes a discontinuous lubricating film.

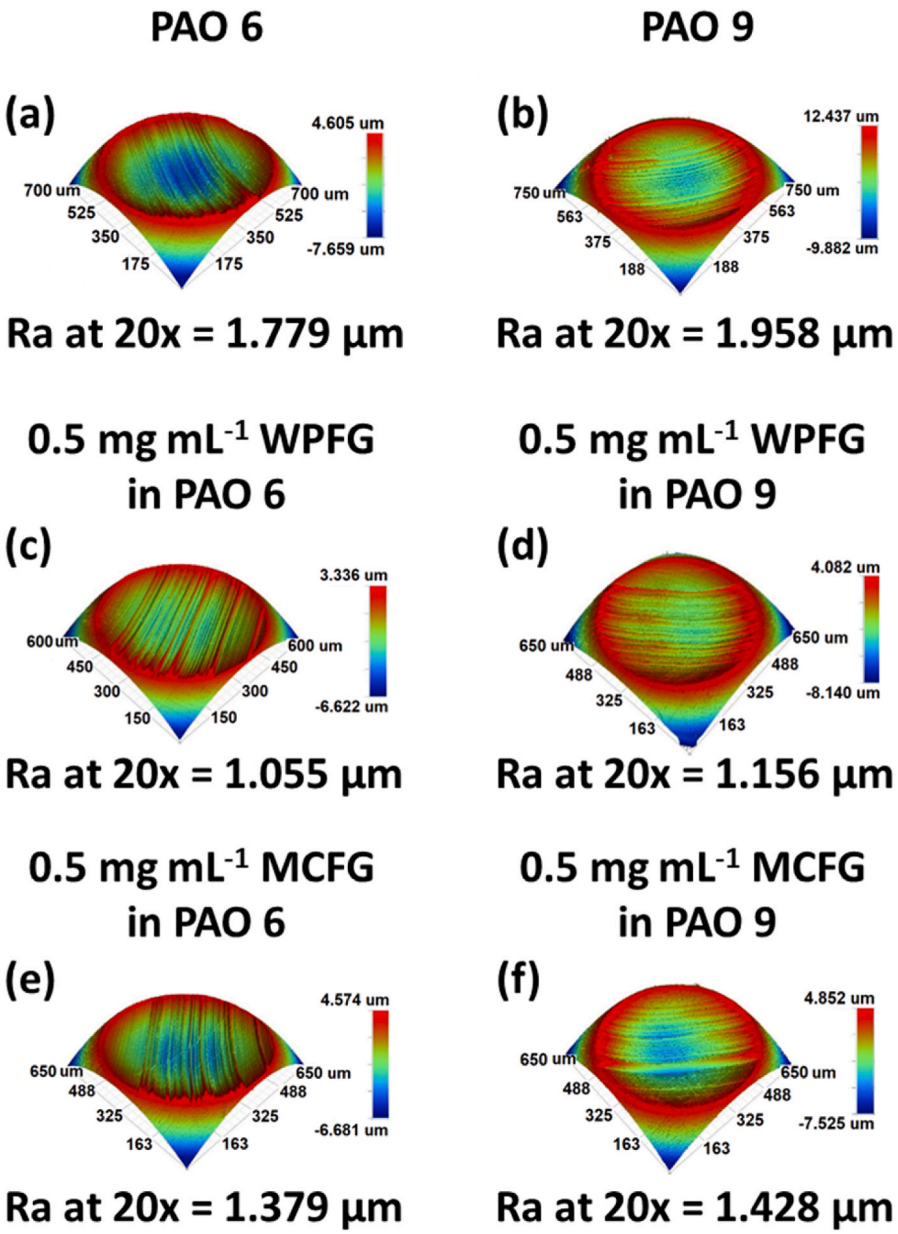

Fig. 6. White light interferometer 3D topographic images of wear scars on steel balls after testing in (a) PAO 6, (b) PAO 9, (c) PAO 6 with 0.5 mg mL^{-1} WPFG, (d) PAO 9 with 0.5 mg mL^{-1} WPFG, (e) PAO 6 with 0.5 mg mL^{-1} MCFG, and (f) PAO 9 with 0.5 mg mL^{-1} MCFG. Ra is the average surface roughness. Images were taken after sonication in an acetone bath for 30 min. (A colour version of this figure can be viewed online.)

It was also found that smaller flakes of WPFG performed better in terms of WSD reduction when compared to the larger flakes of MCFG. This behavior can be explained because smaller particles of WPFG (Avg. Size: 21.3 ± 10.8 nm, Fig. S10) would more easily enter the contact interface to enhance lubrication while maintaining the continuity of the lubricant film, when compared to the larger particles of MCFG (Avg. Size: 780.6 ± 566.4 nm, Fig. S11) [37]. WPFG and MCFG are used here due to the large disparity in flake sizes compared to each other and to CG. WPFG is smaller than CG and MCFG is larger than CG (Avg. Size: 254.5 ± 63.5 nm, Fig. S12) [38], yet as seen previously, both WPFG and MCFG are still more dispersible than CG in both lubricant oils. The turbostraticity of FG enables greater dispersibility of FG, even when MCFG is much larger than the AB-stacked CG. Previous reports have shown that the size of the FG flakes depends greatly on the initial feedstock used for conversion [22] and the parameters used for FJH [2]. As such, varying the feedstock and parameters for FJH is necessary to obtain flakes that are an appropriate size for any given application. Smaller particles, such as those with similar sizes to graphene quantum dots [39] (Avg. Size: 2.96 ± 0.96 nm), will likely perform best due to their ability to enter the contact interface. In addition to this difference in particle size, WPFG appears to consist of smaller particles with several layers stacked on top of one another (Fig. S11), whereas MCFG appears to consist of larger sheet-like flakes (Fig. S11). As such, WPFG and MCFG will likely enter the lubricated contact in the form of particles and sheets, respectively.

Literature has reported the use of other carbon nanofillers as lubricant additives, such as single layer graphene oxide (GO) [40], GO [41], single layer graphene [42], multilayer graphene [43], modified graphene platelets [44], CeO_2-decorated graphene [45], ZrO_2/rGO composites [46], Cu nanoparticles decorated on polydopamine functionalized GO [47], zinc borate/GO composites [48], and silica/GO composites [49]. While these modified materials can obtain comparable or better reductions in CoF and WSD (Table S4) than FG, the GO and graphene precursors of these carbon nanofillers are obtained through physical (GPE) or chemical exfoliation (GCE) of graphite. Preliminary life cycle analyses of MCFG, WPFG, GPE, and GCE [23] shows that preparation of MCFG and WPFG emits fewer greenhouse gases and consumes less water and energy when compared to GPE and GCE (Fig. 7). Compared to production of GPE, production of MCFG and WPFG emit 98.8% and 89.6% less greenhouse gas emissions, respectively. When assessing the energy consumption for production of GPE, production of MCFG and WPFG require 98.4% and 97.0% less energy, respectively. Finally, when compared to GCE, MCFG and WPFG consume 99.9% and 99.2% less water, respectively. The difference in emission, energy consumption, and water consumption only grows larger when one considers the various chemical modifications needed to functionalize non-turbostratic graphene for dispersion in lubricants.

4. Conclusions

FG produced from low- and negative-value feedstocks was used as an additive to PAO 9 and PAO 6 lubricant oils to reduce friction, wear, and surface roughness. The turbostraticity of the WPFG and MCFG makes them up to 14x and 5x more dispersible, respectively, in lubricant oil than AB-stacked CG, making them ideal candidates as additives to lubricants. The FG additives delivered a decrease in CoF of up to 23% and a decrease in WSD of up to 14%. Average roughness was decreased by up to 38%, which means that the surfaces effectively become smoother with the FG additives. Additionally, production of turbostratic FG requires up to 99% less water, 98% less energy, and emits up to 98.8% fewer greenhouse gas emissions when compared to conventional production of AB-stacked graphene. The ease and affordability of FJH as a method for FG synthesis from low- and negative-value feedstocks means that FG can be effectively used on a large scale as a lubricant additive to extend lifetime and reliability of mechanical systems with sliding contacts.

Notes

The authors declare the following competing financial interest(s): Rice University owns intellectual property on the synthesis and use of FG. That intellectual property has been licensed to a company in which JMT is a stockholder, but not an officer, director, or employee. Conflicts of interest are mitigated through regular disclosure to and compliance with the Rice University Office of Sponsored Programs and Research

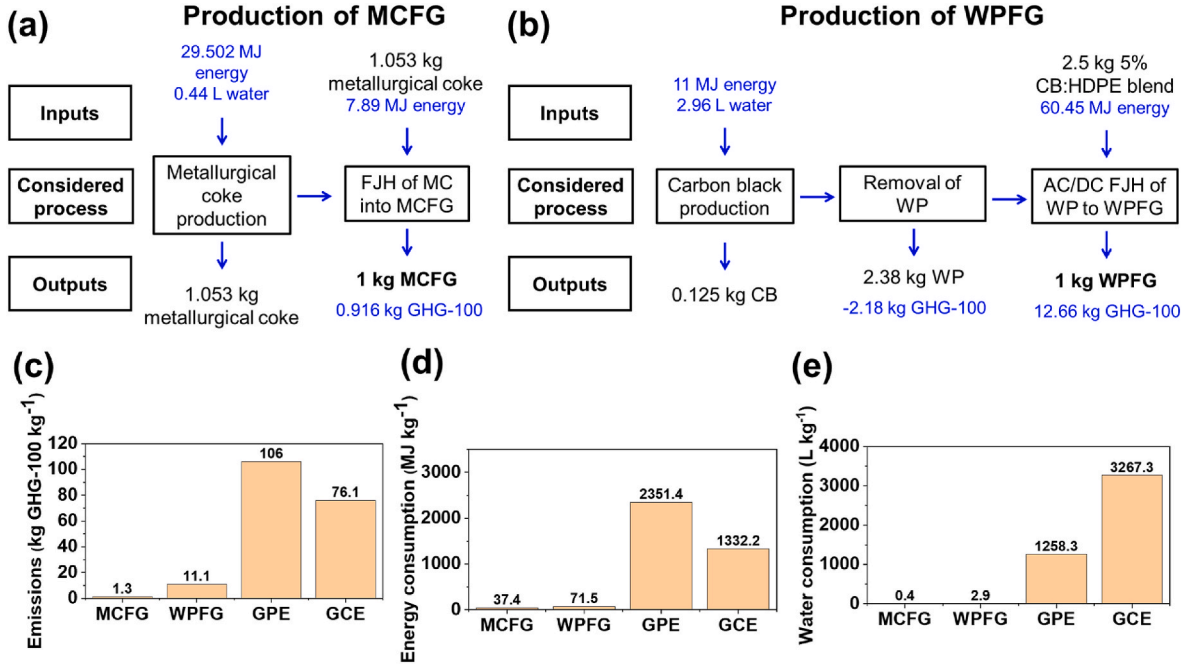

Fig. 7. Flow chart of production of equivalent masses (1 kg) of (a) MCFG and (b) WPFG. Comparison of (e) GHG emissions, (f) energy consumption, and (g) water consumption for production of equivalent masses (1 kg) of MCFG, WPFG, graphene from physical exfoliation (GPE) and graphene from chemical exfoliation (GCE). (A colour version of this figure can be viewed online.)

Compliance. The authors declare no other potential conflicts of interest.

CRediT authorship contribution statement

Paul A. Advincula: Conceptualization, Methodology, Investigation, Writing – original draft. **Victoria Granja:** Investigation, Visualization, Writing – review & editing. **Kevin M. Wyss:** Resources. **Wala A. Algozeeb:** Resources. **Weiyin Chen:** Investigation. **Jacob L. Beckham:** Data curation, Software. **Duy Xuan Luong:** Resources. **C. Fred Higgs:** Supervision, Writing – review & editing. **James M. Tour:** Supervision, Writing – review & editing.

Declaration of competing interest

The authors declare the following financial interests/personal relationships which may be considered as potential competing interests:

James M. Tour reports financial support was provided by Air Force Office of Scientific Research. James M. Tour reports financial support was provided by U S Army Corps of Engineers. Kevin M. Wyss reports financial support was provided by National Science Foundation. Jacob L. Beckham reports financial support was provided by National Science Foundation. Wala A. Algozeeb reports financial support was provided by Saudi Arabian Oil Co.

Acknowledgements

The Air Force Office of Scientific Research (FA9550-22-1-0526), the U.S. Army Corps of Engineers ERDC (W912HZ-21-2-0050), and the DOE-NETL (DE-FE0031794) funded this work. J.L.B. acknowledges support from the NSF Graduate Research Fellowship Program. We thank Saudi Aramco for the fellowship support of W.A.A. We thank Bo Chen for his help with XPS analyses.

Appendix A. Supplementary data

Supplementary data to this article can be found online at https://doi.org/10.1016/j.carbon.2022.12.035.

References

[1] D. Berman, A. Erdemir, A.V. Sumant, Graphene: a new emerging lubricant, Mater. Today 17 (2014) 31–42.
[2] M.G. Stanford, K.V. Bets, D.X. Luong, P.A. Advincula, W. Chen, J.T. Li, Z. Wang, E. A. McHugh, W.A. Algozeeb, B.I. Yakobson, J.M. Tour, Flash graphene morphologies, ACS Nano 14 (2020) 13691–13699.
[3] W. Chen, C. Ge, J.T. Li, J.L. Beckham, Z. Yuan, K.M. Wyss, P.A. Advincula, L. Eddy, C. Kittrell, J. Chen, D.X. Luong, R.A. Carter, J.M. Tour, Heteroatom-doped flash graphene, ACS Nano 16 (2022) 6646–6656.
[4] W. Chen, J.T. Li, Z. Wang, W.A. Algozeeb, D.X. Luong, C. Kittrell, E.A. McHugh, P. A. Advincula, K.M. Wyss, J.L. Beckham, M.G. Stanford, B. Jiang, J.M. Tour, Ultrafast and controllable phase evolution by flash Joule heating, ACS Nano 15 (2021) 11158–11167.
[5] W.A. Algozeeb, P.E. Savas, D.X. Luong, W. Chen, C. Kittrell, M. Bhat, R. Shahsavari, J.M. Tour, Flash graphene from plastic waste, ACS Nano 14 (2020) 15595–15604.
[6] P.A. Advincula, D.X. Luong, W. Chen, S. Raghuraman, R. Shahsavari, J.M. Tour, Flash graphene from rubber waste, Carbon 178 (2021) 649–656.
[7] K.M. Wyss, J.L. Beckham, W. Chen, D.X. Luong, P. Hundi, S. Raghuraman, R. Shahsavari, J.M. Tour, Converting plastic waste pyrolysis ash into flash graphene, Carbon 174 (2021) 430–438.
[8] Universal matter material science: graphene in A flash, n.d. https://www.universalmatter.com/?gclid=Cj0KCQjwm9yJBhDTARIsABKIcGabwLgKN55Hhk_-vOB0xix77WekBB6JH7YDOLk4Jo7O-Pbn1HKLtdkaAq5TEALw_wcB. (Accessed 7 September 2021).
[9] P.A. Advincula, A.C. De Leon, B.J. Rodier, J. Kwon, R.C. Advincula, E.B. Pentzer, Accommodating volume change and imparting thermal conductivity by encapsulation of phase change materials in carbon nanoparticles, J. Mater. Chem. A. 6 (2018) 2461–2467.
[10] S.J. Barnes, Understanding plastics pollution: the role of economic development and technological research, Environ. Pollut. 249 (2019) 812–821.
[11] J. Zheng, S. Suh, Strategies to reduce the global carbon footprint of plastics, Nat. Clim. Change 9 (2019) 374–378.
[12] World Economic Forum, The New Plastics Economy: Rethinking the Future of Plastics, 2016.
[13] D. Lithner, I. Nordensvan, G. Dave, Comparative acute toxicity of leachates from plastic products made of polypropylene, polyethylene, PVC, acrylonitrile-butadiene-styrene, and epoxy to Daphnia magna, Environ. Sci. Pollut. Res. 19 (2012) 1763–1772.
[14] S.G. Tetu, I. Sarker, V. Schrameyer, R. Pickford, L.D.H. Elbourne, L.R. Moore, I. T. Paulsen, Plastic leachates impair growth and oxygen production in Prochlorococcus, the ocean's most abundant photosynthetic bacteria, Commun. Biol. 2 (2019) 1–9.
[15] S. Sharma, S. Chatterjee, Microplastic pollution, a threat to marine ecosystem and human health: a short review, Environ. Sci. Pollut. Res. 24 (2017) 21530–21547.
[16] J.C. Prata, Airborne microplastics: consequences to human health? Environ, Pollut. 234 (2018) 115–126.
[17] K.D. Cox, G.A. Covernton, H.L. Davies, J.F. Dower, F. Juanes, S.E. Dudas, Human consumption of microplastics, Environ. Sci. Technol. 53 (2019) 7068–7074.
[18] NOAA, How Much Oxygen Comes from the Ocean?, 2021, p. 1. June 25, 2022), https://oceanservice.noaa.gov/facts/ocean-oxygen.html.
[19] M. Shen, S. Ye, G. Zeng, Y. Zhang, L. Xing, W. Tang, X. Wen, S. Liu, Can microplastics pose a threat to ocean carbon sequestration? Mar. Pollut. Bull. 150 (2020), 110712.
[20] K. Kvale, A.E.F. Prowe, C.T. Chien, A. Landolfi, A. Oschlies, Zooplankton grazing of microplastic can accelerate global loss of ocean oxygen, Nat. Commun. 12 (2021) 1–8.
[21] IEA, Net Zero by 2050: A Roadmap for the Global Energy Sector, Int. Energy Agency., 2021, p. 224.
[22] D.X. Luong, K.V. Bets, W.A. Algozeeb, M.G. Stanford, C. Kittrell, W. Chen, R. V. Salvatierra, M. Ren, E.A. McHugh, P.A. Advincula, Z. Wang, M. Bhatt, H. Guo, V. Mancevski, R. Shahsavari, B.I. Yakobson, J.M. Tour, Gram-scale bottom-up flash graphene synthesis, Nature 577 (2020) 647–651.
[23] K.M. Wyss, R.D. De Kleine, R.L. Couvreur, A. Kiziltas, D.F. Mielewski, J.M. Tour, Upcycling end-of-life vehicle waste plastic into flash graphene, Commun. Eng. 1 (2022) 3.
[24] J.L. Beckham, K.M. Wyss, Y. Xie, E.A. McHugh, J.T. Li, P.A. Advincula, W. Chen, J. Lin, J.M. Tour, Machine learning guided synthesis of flash graphene, Adv. Mater. 34 (2022), 2106506.
[25] H.W.J. Dias, A.B. Medeiros, C. Binder, J.B.R. Neto, A.N. Klein, J.D.B. de Mello, Tribological evaluation of turbostratic 2d graphite as oil additive, Lubricants 9 (2021) 43.
[26] ASTM International, ASTM D4172-20, Standard Test Method for Wear Preventive Characteristics of Lubricating Fluid, Four-Ball Method), West Conshohocken, PA, 2020.
[27] B.J. Hamrock, D. Dowson, Isothermal elastohydrodynamic lubrication of point contacts: Part III-fully flooded result, J. Tribol. 99 (1977) 264–275.
[28] Z.Q. Li, C.J. Lu, Z.P. Xia, Y. Zhou, Z. Luo, X-ray diffraction patterns of graphite and turbostratic carbon, Carbon 45 (2007) 1686–1695.
[29] W. Zhang, M. Zhou, H. Zhu, Y. Tian, K. Wang, J. Wei, F. Ji, X. Li, Z. Li, P. Zhang, D. Wu, Tribological properties of oleic acid-modified graphene as lubricant oil additives, J. Phys. D Appl. Phys. 44 (2011), 205303.
[30] J. Williams, Engineering Tribology, Cambridge University Press, 2005.
[31] H.J. Song, X.H. Jia, N. Li, X.F. Yang, H. Tang, Synthesis of α-Fe_2O_3 nanorod/graphene oxide composites and their tribological properties, J. Mater. Chem. 22 (2012) 895–902.
[32] Y. Meng, F. Su, Y. Chen, Supercritical fluid synthesis and tribological applications of silver nanoparticle-decorated graphene in engine oil nanofluid, Sci. Rep. 6 (2016) 1–12.
[33] Y. Liu, X. Ge, J. Li, Graphene lubrication, Appl. Mater. Today 20 (2020), 100662.
[34] Y. Wu, X. Zeng, T. Ren, E. de Vries, E. van der Heide, The emulsifying and tribological properties of modified graphene oxide in oil-in-water emulsion, Tribol. Int. 105 (2017) 304–316.
[35] H. Kinoshita, M. Kondo, Y. Nishina, M. Fujii, Anti-wear effect of graphene oxide in lubrication by fluorine-containing ionic liquid for steel, Tribol. Online 10 (2015) 91–95.
[36] V. Zin, F. Agresti, S. Barison, L. Colla, M. Fabrizio, Influence of Cu, TiO_2 nanoparticles and carbon nano-horns on tribological properties of engine oil, J. Nanosci. Nanotechnol. 15 (2015) 3590–3598.
[37] P.L. Menezes, M.R. Lovell, M.A. Kabir, C.F. Higgs, P.K. Rohatgi, Green lubricants: role of additive size, Green Energy Technol. 49 (2012) 265–286.
[38] Graphene powder – graphene product| Tianyuan Empire, n.d. http://www.ty-empire.com/graphene-products/graphene-powder/?lang=en. (Accessed 4 October 2022).
[39] R. Ye, C. Xiang, J. Lin, Z. Peng, K. Huang, Z. Yan, N.P. Cook, E.L.G. Samuel, C. C. Hwang, G. Ruan, G. Ceriotti, A.R.O. Raji, A.A. Martí, J.M. Tour, Coal as an abundant source of graphene quantum dots, Nat. Commun. 4 (2013) 1–7.
[40] A. He, S. Huang, J.H. Yun, Z. Jiang, J. Stokes, S. Jiao, L. Wang, H. Huang, The pH-dependent structural and tribological behaviour of aqueous graphene oxide suspensions, Tribol. Int. 116 (2017) 460–469.
[41] A. Senatore, V. D'Agostino, V. Petrone, P. Ciambelli, M. Sarno, Graphene oxide nanosheets as effective friction modifier for oil lubricant: materials, methods, and tribological results, ISRN Tribol. 2013 (2013) 1–9.
[42] D. Marchetto, P. Restuccia, A. Ballestrazzi, M.C. Righi, A. Rota, S. Valeri, Surface passivation by graphene in the lubrication of iron: a comparison with bronze, Carbon 116 (2017) 375–380.
[43] X. Fan, Y. Xia, L. Wang, W. Li, Multilayer graphene as a lubricating additive in bentone grease, Tribol. Lett. 55 (2014) 455–464.
[44] J. Lin, L. Wang, G. Chen, Modification of graphene platelets and their tribological properties as a lubricant additive, Tribol. Lett. 41 (2011) 209–215.

[45] G. Bai, J. Wang, Z. Yang, H. Wang, Z. Wang, S. Yang, Preparation of a highly effective lubricating oil additive-ceria/graphene composite, RSC Adv. 4 (2014) 47096–47105.
[46] Q. Zhou, J. Huang, J. Wang, Z. Yang, S. Liu, Z. Wang, S. Yang, Preparation of a reduced graphene oxide/zirconia nanocomposite and its application as a novel lubricant oil additive, RSC Adv. 5 (2015) 91802–91812.
[47] H. Song, Z. Wang, J. Yang, X. Jia, Z. Zhang, Facile synthesis of copper/polydopamine functionalized graphene oxide nanocomposites with enhanced tribological performance, Chem. Eng. J. 324 (2017) 51–62.
[48] Z.L. Cheng, W. Li, Z. Liu, Preparation, characterization, and tribological properties of oleic diethanolamide-capped zinc borate-coated graphene oxide composites, J. Alloys Compd. 705 (2017) 384–391.
[49] V.K. Singh, O. Elomaa, L.S. Johansson, S.P. Hannula, J. Koskinen, Lubricating properties of silica/graphene oxide composite powders, Carbon 79 (2014) 227–235.